scientific reports

Check for updates

OPEN

Machine learning algorithms and artificial neural networks for predicting schizophrenia using orbital parameters

Elif Emre[1], Derya Ozturk Soylemez[2], Yusuf Secgin[3], Seda Sogukpinar Karaagac[4], Omer Kenanoglu[5] & Suleyman Aydin[6]✉

A persistent mental illness, schizophrenia has a complicated etiopathogenesis that includes both environmental and genetic elements. This study examined the possibility of diagnosing schizophrenia by utilizing computed tomography (CT) images of the orbit and its structures, which were then examined by artificial neural networks (ANNs) and machine learning (ML) algorithms. A retrospective analysis of the CT scans of 90 healthy people and 90 people with schizophrenia was conducted. Prior to measurement, all CT images underwent preprocessing steps to ensure align-ment and standardization. Height, width, depth, wall length, aperture area, interorbital width, biorbital width, bimalar width, skull transverse diameter, and optic nerve sheath width were among the orbital parameters that were measured. Statistical analysis revealed significant differences between the groups in left orbital width, left orbital aperture area, right optic nerve sheath width, transverse skull diameter, bimalar width, biorbital width, and left medial wall length. ML algorithms and ANNs were applied to the data, with the Extra Tree Classifier (ETC) algorithm achieving the highest accuracy of 0.78 and the Multilayer Perceptron Classifier (MLCP) model of ANN achieving an accuracy of 0.75 after 1000 training iterations. The Random Forest algorithm's SHAP analyzer determined that the left orbital width had the biggest impact on the final outcome. These results add to the expanding field of machine learning applications in psychiatry by indicating that AI-based models that analyze orbital morphometry may be useful instruments for detecting schizophrenia.

Keywords Schizophrenia, Computed tomography, Machine learning, Artificial neural networks, Orbital parameters

Since ancient times, anthropometric measures taken in line with specific criteria in the human body have been systematically examined to assess an individual's growth and development status and identify correlations with different disorders[1]. Anthropometric measurements have been used for many years to diagnose a wide range of disorders and identify risk factors[2–4]. Anthropometric measurement evaluation has entered a new era with the advancement of computer technology and imaging techniques in the medical area[5].

Certain morphometric parameters, including nasal root depth, upper lip height, and forehead slope, are known to vary among patients with schizophrenia and other structural alterations in cerebral morphology[6]. In studies using magnetic resonance imaging (MRI), decreased frontal lobe volume, hippocampal atrophy, enlargement of the lateral and third ventricles, and temporomlimbic abnormalities are among the most frequently reported findings of schizophrenia. Functional MRI studies have revealed functional connectivity abnormalities and activity changes in the dorsolateral prefrontal cortex, anterior cingulate cortex, and temporoparietal regions[7]. In addition to brain imaging, optical coherence tomography (OCT) has been used to show decreased nerve fiber layer thickness in the retina and cornea, particularly in the orbitofrontal cortex. It has also been used to show changes in retinal microvascular structures, such as decreased vascular density around the fovea[8].

[1]Department of Anatomy, Faculty of Medicine, Firat University, Elazig, Turkey. [2]Vocational School of Health Services, Sinop University, Sinop, Turkey. [3]Department of Anatomy, Faculty of Medicine, Karabük University, Karabük, Turkey. [4]Department of Radiology, Faculty of Medicine, Firat University, Elazig, Turkey. [5]Department of Psychiatry, Faculty of Medicine, Dicle University, Diyarbakir, Turkey. [6]Department of Medical Biochemistry (Firat Hormone Research Group), Faculty of Medicine, Firat University, Elazig, Turkey. ✉email: saydin1@hotmail.com

Schizophrenia is a long-term mental illness that typically begins in adolescence or early adulthood and is defined by anomalies in motor skills, cognitive and emotional functioning, and cognition and perception[9]. Numerous environmental and neurodevelopmental variables, particularly genetic ones, have been identified, despite the fact that its etiopathogenesis is still unclear[10,11]. Certain phenotypic traits and mental disorders are linked to genetic and environmental variables during prenatal development[12,13]. The nervus opticus and bulbus oculi are considered continuations of the brain, and the orbital cavity in which they are located is in close anatomical proximity to critical structures such as the paranasal sinuses, intracranial cavity, and facial bones. These regions can be affected by various pathological conditions, including sinusitis, orbital cellulitis, tumors, trauma, and congenital or developmental anomalies in adjacent brain tissues (frontal lobe, temporal lobe, cranial nerves)[14,15]. The orbital cavity's anatomical structure may be impacted by structural alterations in schizophrenia patients, including a de-crease in frontal lobe volume (especially in the orbitofrontal cortex), abnormalities of the temporolimbic region, and thinning of the cornea and retinal nerve fiber layer[7,8].

As technology has advanced in recent years, artificial intelligence has started to be applied in a variety of disciplines, including health. Medical picture interpretation and pathology identification can be aided by machine learning (ML) techniques[2]. Logistic regression is a linear method that models the relationship between input variables and a binary outcome in terms of probability. The Extra Tree Classifier combines multiple decision trees built with randomly selected splits, producing fast and generalizable results. Linear Discriminant Analysis (LDA) identifies linear boundaries that best separate classes, whereas Quadratic Discriminant Analysis (QDA) allows different covariance structures, resulting in quadratic decision boundaries. A Decision Tree classifies data by recursively splitting it into branches, while a Random Forest aggregates multiple trees to achieve more stable and accurate predictions. Gaussian Naive Bayes assumes feature independence and normal distribution within classes, offering a simple and efficient classification approach. The k-Nearest Neighbors (kNN) algorithm classifies samples based on the proximity of neighboring instances. The Multi-Layer Perceptron (MLP) employs a multi-layer neural network structure capable of learning complex, nonlinear relationships within data[16].

Computed tomography (CT) is a radiological technique that can visualize all tissues, especially bone tissue. Also, it has been reported that the optic nerve head tomographic characteristics of individuals with schizophrenia differ from those of healthy participants Further-more, the mean relative ventricular volumes for the anterior, lateral, and temporal horns were higher in patients with schizophrenia[17]. As demonstrated above, structural neuroimaging studies (such as orbital subregions) have provided the most trustworthy evidence of brain anomalies in schizophrenia[18,19]. Little is known about the use of orbital morphometry in schizophrenia, and prior magnetic resonance imaging (MRI) results from orbitofrontal cortex (OFC) volume studies have been conflicting, with some suggesting decreased OFC volume in schizophrenia compared with controls. Individual differences in cognitive function (such as abstract thought, decision-making, and perceptual organization), psychiatric symptomatology (such as hallucinations, psychomotor excitement, disorganized symptoms, anhedonia, and social deficits), and personality traits (such as impulsivity or apathy) may all be reflected in the variation in OFC sulcogyral pattern (Figs. 1 and 2).

In order to diagnose schizophrenia, the current study sought to ascertain whether machine learning algorithms and artificial neural networks might be utilized to evaluate the orbit's characteristics and structures as indicated by CT images.

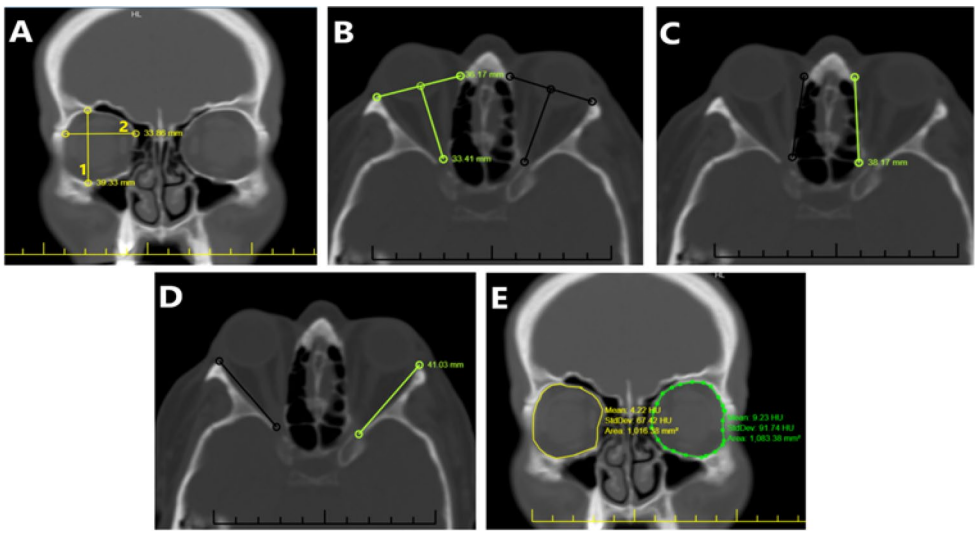

Fig. 1. Demonstration of measurement parameters. (**A**) Height of the orbit, (**B**) Depth of the orbit, (**C**) Medial wall length of the orbit, (**D**) Lateral wall length of the orbit, (**E**) Orbital aperture area, (**A** and **E**) are images in the coronal section, (**B**, **C**, and **D**) are images in the axial section).

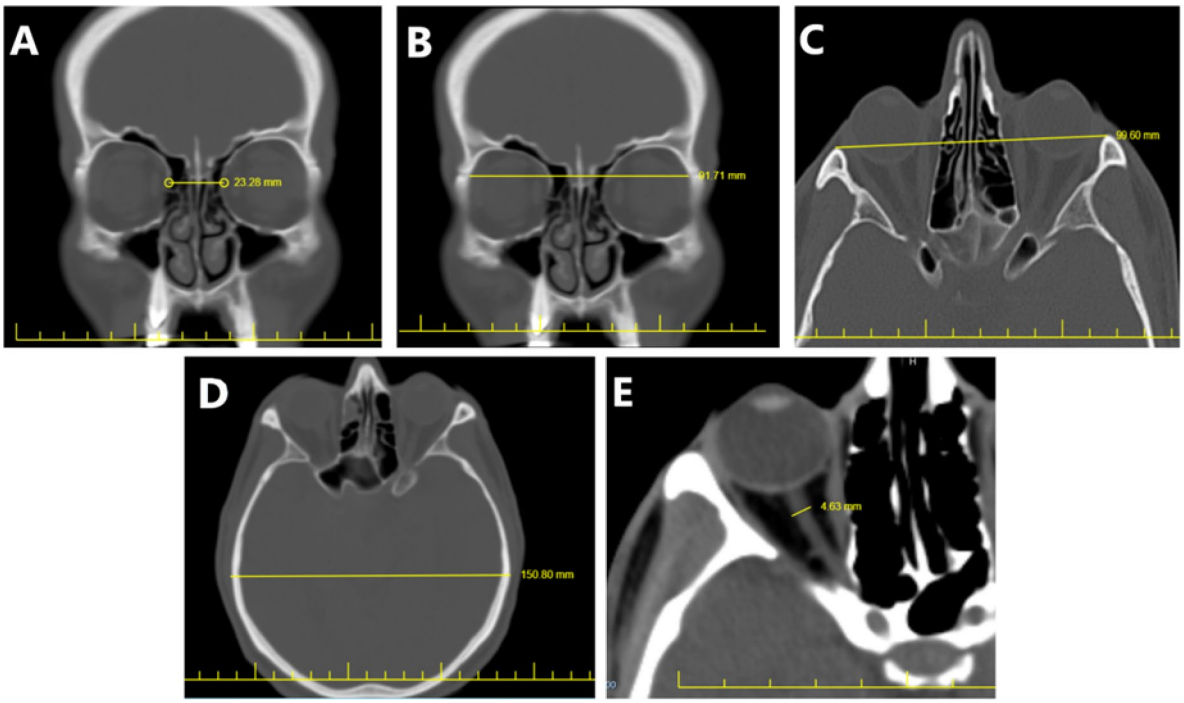

Fig. 2. Demonstration of measurement parameters (**A**) Interorbital width, (**B**) Biorbital width, (**C**) Bimalar width; (**D**) Skull transverse diameter; (**E**) Optic nerve-sheath width, (**A** and **B**) are images in the coronal section, (**C**, **D**, and **E**) are images in the axial section).

Parameters	Group	Mean ± standard deviation	p^*
Width of the left orbit	Control	34.779 ± 2.027	**0.001**
	Schizophrenia	33.565 ± 1.855	
Depth of the right orbit	Control	37.962 ± 3.220	0.752
	Schizophrenia	38.107 ± 2.930	
Length of the lateral walls of the right orbit	Control	41.243 ± 3.067	0.113
	Schizophrenia	41.967 ± 3.032	
Length of the lateral walls of the left orbit	Control	40.731 ± 3.433	0.058
	Schizophrenia	41.632 ± 2.861	
Right optic nerve-sheath width	Control	5.557 ± 0.689	**0.025**
	Schizophrenia	5.323 ± 0.706	
Skull transverse diameter	Control	141.16 ± 8.53	**0.029**
	Schizophrenia	138.74 ± 6.03	

Table 1. Group comparisons and descriptive statistics for data that is regularly distributed. *Two sample T test. Significant values are in bold.

Results

In this study, 90 healthy individuals without schizophrenia (control group) and 90 individuals with schizophrenia (schizophrenia group), the width of the left orbit, depth of the right orbit, length of the lateral walls of the right orbit, length of the lateral walls of the left orbit, right optic nerve-sheath width, skull transverse diameter parameters were found to be normally distributed, and left orbit width, right optic nerve sheath width, and skull transverse diameter parameters were significantly different between the groups (Table 1) ($p < 0.05$).

Descriptive statistics and group comparisons of parameters that did not show a normal distribution are shown in Table 2. The length of the medial walls of the orbit, left orbital aperture area, bimalar width, and biorbital width were found to be significantly different between the groups ($p < 0.05$). In addition, there was no significant difference between the groups in terms of age ($p > 0.05$); the age distribution of the schizophrenia group was 44 (29–64 year) and the control group was 47.50 (29–64 year).

As a result of the analysis of ML algorithms with 20% of the data as a test set, the highest Acc rate was found to be 0.78 with the ETC algorithm (Table 3). The ETC algorithm with the highest accuracy rate correctly predicted 14 of the 18 individuals in the control group and 14 of the 18 individuals in the schizophrenia group in the test

Parameters	Group	Median (min–max)	*p***
Width of the right orbit	Control	34.655 (29.470–42.100)	0.079
	Schizophrenia	33.935 (30.640–40.000)	
Height of the right orbit	Control	39.130 (32.940–53.500)	0.058
	Schizophrenia	38.820 (33.030–46.930)	
Height of the left orbit	Control	39.505 (34.970–69.800)	0.326
	Schizophrenia	38.745 (33.640–46.610)	
Depth of the left orbit	Control	37.745 (29.050–54.700)	0.207
	Schizophrenia	38.765 (31.620–45.660)	
Length of the medial walls of the right orbit	Control	41.345 (30.050–50.400)	0.241
	Schizophrenia	42.155 (35.510–63.180)	
Length of the medial walls of the left orbit	Control	40.640 (28.300–74.160)	**0.002**
	Schizophrenia	42.685 (36.980–51.030)	
Right orbital aperture area	Control	1093.2 (826.7–1396.0)	0.058
	Schizophrenia	1058.9 (897.4–1288.5)	
Left orbital aperture area	Control	1081.6 (126.5–1340.1)	**0.001**
	Schizophrenia	1041.5 (127.3–1269.8)	
Bimalar width	Control	97.725 (86.800–105.440)	**0.020**
	Schizophrenia	96.345 (69.560–105.370)	
Biorbital width	Control	94.830 (83.230–102.860)	**0.015**
	Schizophrenia	93.12 (82.01–102.05)	
Interorbital width	Control	25.100 (19.560–36.840)	0.350
	Schizophrenia	24.63 (18.99–48.13)	
Left optic nerve-sheath width	Control	5.310 (4.040–7.370)	0.613
	Schizophrenia	5.190 (3.590–8.490	

Table 2. Group comparisons and descriptive statistics for data that is not regularly distributed. **Mann Whitney U test. Significant values are in bold.

Algorithms	Accuracy	Specificity	Sensitivity	F1 score
Logistic regression	0.72	0.72	0.72	0.72
Extra tree classifier	0.78	0.78	0.78	0.78
Linear discriminant analysis	0.72	0.72	0.72	0.72
Quadratic discriminant analysis	0.75	0.75	0.75	0.75
Decision tree	0.58	0.61	0.58	0.56
Random forest	0.72	0.72	0.72	0.72
Gaussian Naive Bayes (Gaussian NB)	0.72	0.72	0.72	0.72
k-nearest neighbors (k = 5)	0.61	0.64	0.61	0.59

Table 3. Machine learning algorithm results (20% test set).

set (Fig. 3A). The ROC curve of the ETC algorithm with the highest Acc rate is shown in Fig. 3B). Using the SHAP analyzer of the RF algorithm, the effect of the parameters on the overall result was evaluated, and it was found that the width of the left orbit had the greatest effect (Fig. 4).

In addition, in our study, the data were also analyzed with ML algorithms by applying tenfold cross validation and the highest Acc rate was found to be 0.74 ± 0.049 with the ETC algorithm (Table 4). The highest Acc rate with the MLCP model of ANN was found to be 0.75 with 1000 times training (Table 5). In the training of the MLCP model 1000 times, 15 of the 18 individuals in the control group and 14 of the 18 individuals in the schizophrenia group in the test set were correctly predicted (Fig. 5A). The model accuracies of the MLCP model during 1000 times training are seen in Fig. 5B.

In this study, the Conditional Tabular Generative Adversarial Network (CTGAN) methodology, which is a synthetic data generation method, was used to observe changes in accuracy values that may arise from a lack of data, and "*n*" synthetic data points were generated. The newly generated dataset was retrained with a 20% test set, and the highest accuracy rate was found to be 0.78 using the ETC algorithm among ML algorithms. The ANN's MLCP model also showed an accuracy of 0.78 after 1000 training sessions (Table 6). The ROC curve for these results and the confusion matrix table for high n models are shown in Fig. 6.

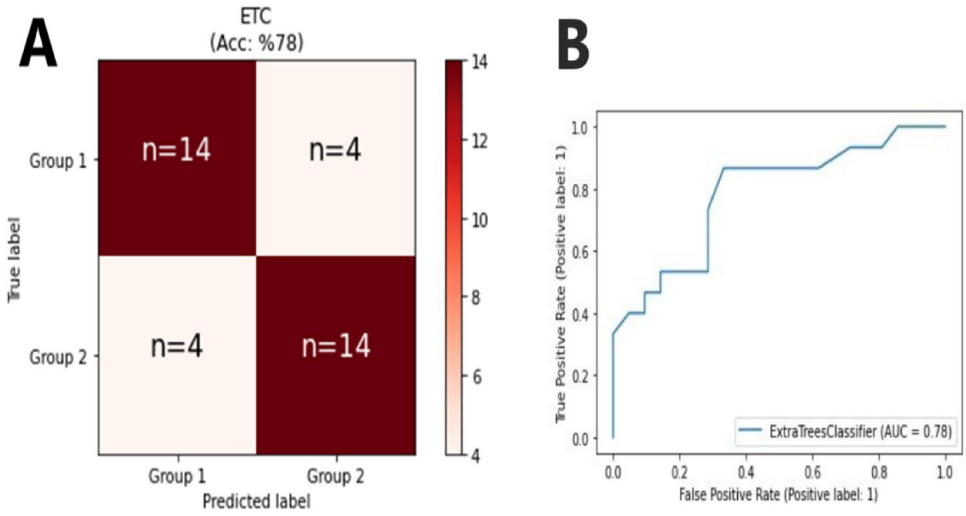

Fig. 3. (**A**) Confusion matrix table for the Extra Tree Classifier algorithm (Group 1 Schizophrenia, Group 2 Control) (20% test set) and (**B**) ROC curve of the ETC algorithm.

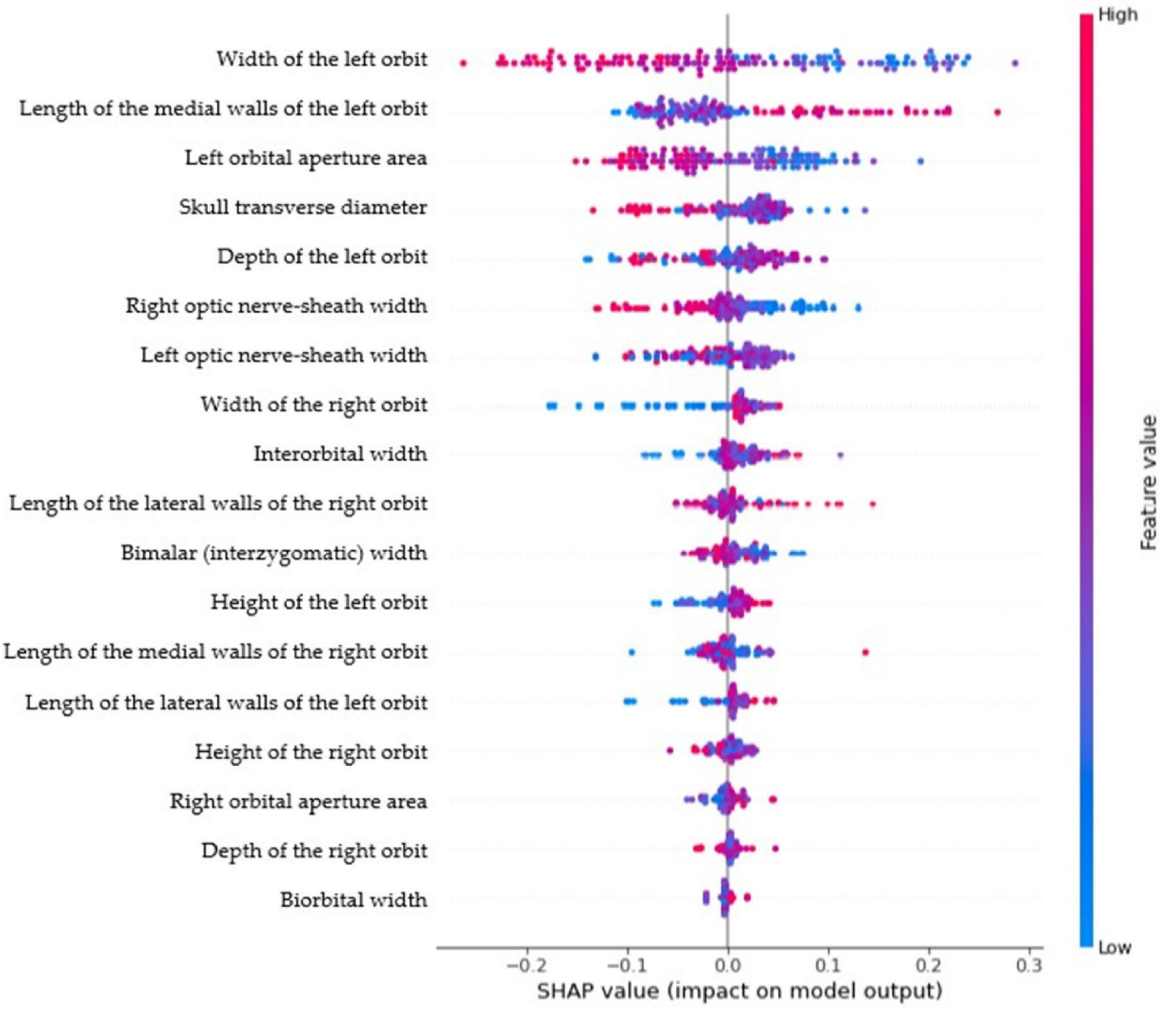

Fig. 4. Shapley Additive explanations (SHAP) solver of the Random Forest algorithm.

Fold sets	LR	ETC	LDA	QDA	DT	RF	GaussianNB	k-NN
1	0.78	0.76	0.78	0.67	0.78	0.67	0.72	0.78
2	0.67	0.76	0.67	0.72	0.56	0.67	0.72	0.56
3	0.72	0.72	0.72	0.67	0.67	0.79	0.67	0.67
4	0.72	0.83	0.72	0.78	0.56	0.60	0.61	0.56
5	0.78	0.67	0.67	0.67	0.56	0.79	0.72	0.56
6	0.78	0.78	0.72	0.78	0.61	0.71	0.67	0.61
7	0.61	0.67	0.69	0.67	0.61	0.79	0.67	0.61
8	0.67	0.72	0.72	0.72	0.39	0.71	0.72	0.39
9	0.72	0.76	0.72	0.72	0.67	0.71	0.72	0.67
10	0.72	0.72	0.67	0.67	0.50	0.60	0.72	0.56
Mean	0.72	0.74	0.71	0.71	0.59	0.71	0.68	0.60
Std	0.056	0.049	0.034	0.048	0.106	0.072	0.048	0.102

Table 4. Results from a machine learning algorithm (tenfold cross validation). Std: Standard deviation.

Number of trainings	Accuracy	Specificity	Sensitivity	F1 score
100	0.72	0.72	0.72	0.72
500	0.72	0.73	0.72	0.72
1000	0.75	0.75	0.75	0.75

Table 5. Analysis of groups with artificial neural networks.

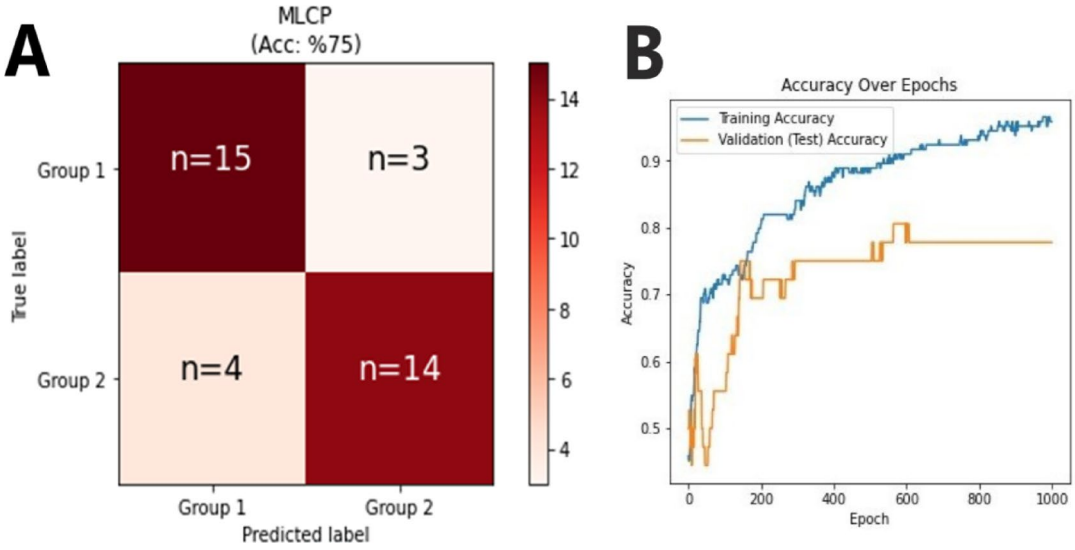

Fig. 5. (**A**) Confusion matrix table for 1000 times learning of the MLCP model (Group 1 Schizophrenia, Group 2 Control), (**B**) accuracies of the MLCP model during 1000 times training.

Discussion

For the first time, machine learning methods and artificial neural networks were used in this study to assess the orbit's anthropometric characteristics and its architecture. According to the results, AI-based models may one day be used to diagnose schizophrenia. Specifically, the ANN-based MLCP model attained an accuracy of 75% in 1000 training repetitions, while the ETC algorithm was the most effective model with an accuracy of 0.78. Given the small number of orbital morphometry-based artificial intelligence applications, the obtained accuracy rates significantly add to the body of knowledge.

According to the statistical analysis, patients with schizophrenia had significantly longer left medial wall lengths and significantly shorter left orbital widths, left orbital aperture areas, right optic nerve-sheath widths, transverse skull diameters, and bimalar and biorbital widths. In a similar study, Keser et al. found that the left orbital height of schizophrenia patients was higher, and the right orbital lateral wall length, left orbital lateral wall length, and left orbital medial wall length values were lower than those in control group[20]. Although similar

Algorithms	Accuracy	Specificity	Sensitivity	F1 score
Logistic regression	0.72	0.72	0.72	0.72
Extra tree classifier	0.78	0.78	0.78	0.78
Linear discriminant analysis	0.72	0.72	0.72	0.72
Quadratic discriminant analysis	0.67	0.67	0.67	0.67
Decision tree	0.64	0.64	0.64	0.64
Random forest	0.72	0.72	0.72	0.72
Gaussian Naive Bayes (GaussianNB)	0.67	0.67	0.67	0.67
k-nearest neighbors (k = 5)	0.65	0.65	0.65	0.65
MLCP (100 times training)	0.78	0.78	0.78	0.78

Table 6. Machine learning algorithm for data processed with CTGAN and MLCP training results 1000 times (20% test set).

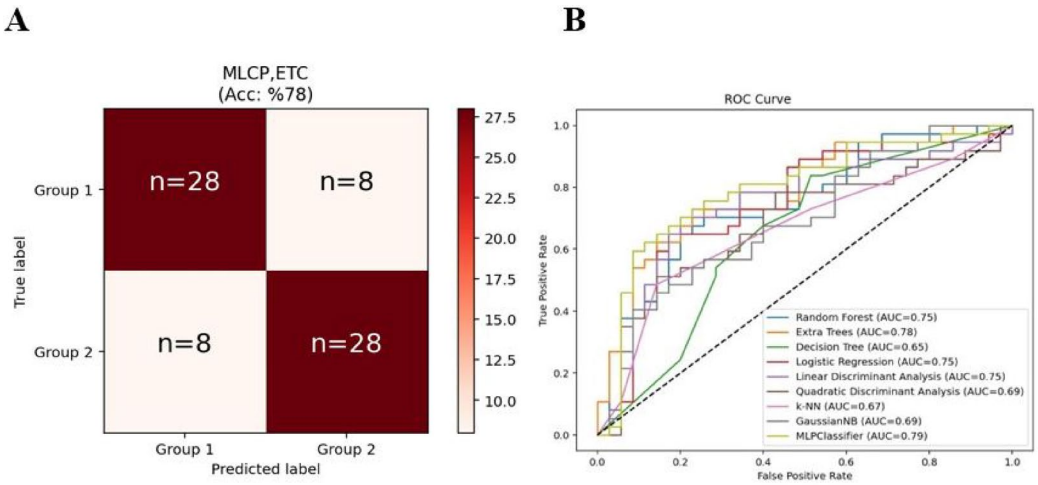

Fig. 6. (**A**) Confusion matrix table of algorithms with the highest accuracy rate in the GTGAN-applied dataset, (**B**) ROC curves of all models in the GTGAN-applied dataset.

parameters were measured, the fact that significant differences were found in different parameters suggests that a single orbital parameter may not be meaningful in making a diagnosis of schizophrenia and that a possible diagnosis may be possible with a more systematic evaluation. According to meta-analyses, schizophrenia is linked to aberrant gyrification patterns, reduced grey matter volumes and cortical thickness, and faster grey matter loss over time. These findings imply that reduced synapse density in specific brain areas is linked to schizophrenia[21]. Consequently, it is crucial to conduct a thorough assessment of artificial neural networks and machine learning algorithms.

Hypertelorismus ocularis, or a wide space between the two eyes, was observed in patients with schizophrenia, according to a 2001 MRI research[22]. When the biorbital length was analyzed, patients with schizophrenia were significantly shorter than those in the control group. Additionally, Keser et al. did not discover any noteworthy variations in interorbital or biorbital lengths[20]. Variations in the enrolled population could be the cause of this disparity. The average age of our registered participants is 46.5 years, which supports this idea, whereas the age of the Keser study sample is 53.7 years. Another difference may be in methodology; in this case, we apply machine learning and artificial intelligence techniques, whereas others merely use the results of row MR images. Also, an intrauterine second-trimester developmental abnormality may be indicated by a small skull size[23]. According to certain research, developmental problems in the second trimester may be linked to schizophrenia[24]. The developmental idea is supported by the fact that the transverse diameter of the skull in our study was substantially less than that of the control group.

Machine learning for psychiatric disorders, particularly schizophrenia, has gained momentum as a promising way to improve diagnosis, prognosis, and understanding of the underlying neurophysiological mechanisms[25]. Machine learning algorithms auto-mate the monitoring of changes in data models using trained learning algorithms[26]. Traditional methods often rely on population-based analysis. In contrast, machine learning is particularly important because it facilitates the development of individualized biomarkers for diseases or functional brain states[27]. The use of neuroimaging data, particularly functional connectivity derived from magnetic resonance imaging, offers a unique opportunity to analyze the complex structures associated with schizophrenia[25,28]. The ability of machine learning to analyze large datasets and identify complex patterns makes it a powerful tool for medical applications[29]. Combining the prior result with the findings of our current study

could potentially save time when diagnosing schizophrenia using machine-learning (ML) techniques that make use of orbital morphometric features. Also, anatomical orbital characteristics (such as dimensions, volume, angles, and distances between anatomical landmarks of the eye orbit) are typically numerical and structured, which are ideal for most machine-learning algorithms for predicting the presence, progression, or success of a diseases.

Zhang et al. developed a deep learning model using brain MRI images of 437 healthy and 450 schizophrenia patients and were able to distinguish schizophrenia patients with 0.96 accuracy, 0.974 sensitivity and 0.944 specificity[30]. In our study, as a result of the MLCP model of the ANN, an accuracy rate of 0.75 was obtained in 1000 iterations of training. In the literature, we did not find any studies examining the orbital parameters of schizophrenia patients using machine-learning methods. However, sex estimation is frequently performed using similar algorithms and different anatomical measurements. Şenol et al. found the highest result in the evaluation of mandibular lingula with ANN for gender prediction with an accuracy rate of 0.81 in 500 training sessions[31]. In another study conducted in 2024, they predicted gender with an accuracy rate between 83 and 86% using DT, LR, RF, LDA, K-Nearest Neighbor and Naive Bayes algorithms with orbital parameters[32]. Triantafyllou et al. 2024 evaluated some parameters of the optic canal in addition to orbital orbital height-width, intraorbital, and extraorbital distance, but obtained a test accuracy of 0.68 with the RF algorithm[33]. In our study, we found that the RF algorithm could diagnose schizophrenia with a sensitivity of 72% using the SHAP analyzer. In this algorithm, the left orbital width had the highest effect, followed by the me-dial wall length of the left orbit and orbital aperture area. Over all, SHAP can help physicians identify biomarkers or other pertinent characteristics in schizophrenia and may offer clear and personalized explanations of which features (e.g., brain areas) are involved.

Considering that many diseases are caused by pathologies in tissues, organs, or neural systems in the human body, analyzing the data obtained with advanced imaging methods using computer algorithms can significantly facilitate the diagnostic process[34]. Our investigation was hampered by the small number of patients. However, even with fewer samples, AI can filter out unnecessary data and convert the remaining data into a more useful format. So that we think that the small number of participants won't have a big effect on our findings. Also, this study was a single-center study, and the fact that the severity of schizophrenia was not assessed by examining each patient separately.

Another disadvantage of the current study is the absence of cross-validations and demographic matching. Also, future research should take into account the limitations of this study, such as data imbalance, retrospective design, and lack of cross-site validation. Despite the aforementioned drawback, our present investigation indicated that the ETC algorithm's 78% accuracy in diagnosing schizophrenia and the ANN's MLCP model's 75% accuracy in diagnosing schizophrenia after 1000 training sessions are crucial for directing doctors. As technology advances and more patient groups are studied, we think that schizophrenia, like many other disorders, may eventually be diagnosed using anthropometric measurements.

Materials and methods

Ethical permissions and study population

The study was approved by the decision numbered 2025/08–17 (session date: 22.05.2025) of the Firat University Non-Interventional Local Ethics Committee. This retrospective study evaluated (5.31. 2023–5.31. 2025) computed tomography (CT) images of 90 healthy individuals without any psychiatric or neurological disease diagnosis (control group: 57 males, 33 females) and 90 individuals diagnosed with schizophrenia (schizophrenia group: 53 males, 37 females), aged between 29 and 64 years, all of which were retrieved from the PACS (picture and communication system) archives. Before being analyzed, every image was completely anonymized, and no identifying clinical or personal information was processed or accessible. Since this retrospective study was conducted using previously collected imaging data, no direct patient contact occurred. The informed consent was waived by Firat University Non-Interventional Local Ethics Committee. The Declaration of Helsinki and institutional data protection rules were followed when conducting the study.

The CT images were obtained using a 256-slice computed tomography machine (General Electric Health Care-Revolution CT, USA). The imaging parameters used in the examinations were as follows: Kv = 120, mA = 200, rotation time = 0.5 s; collimation = 64 × 0.625. Images were transferred to a workstation (DOSEWATCH, General Electric HealthCare, USA) and analyzed. Patients with schizophrenia and healthy individuals with comorbidities, eye diseases, trauma, or surgery in the head region were excluded from this study. In addition, patients with poor-quality CT images, those with any detect-able pathology, those with orbital growth still ongoing (under 18 years of age), and those with significant axial or rotational misalignment on imaging were excluded.

To reduce geometric variability resulting from head rotation or tilt during CT acquisition, all scans were spatially registered to a common reference frame prior to morphometric measurements. This registration was executed using 3D Slicer v5.4 (open-source software, https://www.slicer.org) through a rigid-body transformation (6 degrees of freedom), which corrects for translational and rotational discrepancies without modifying anatomical dimensions.

The anterior commissure–posterior commissure (AC–PC) line and the midsagittal plane were used as anatomical reference landmarks. All images were resampled to an isotropic voxel size of 0.5 × 0.5 × 0.5 mm using bilinear interpolation. Following registration, the orbital region was extracted within a standardized bounding box to ensure a consistent field of view and scaling across all subjects. This preprocessing step ensured that the observed variations in orbital parameters reflected true anatomical differences rather than acquisition-related positional artifacts.

Measurement parameters

Keser and her colleagues provided an explanation of the below measured parameters[20]. No size reduction was performed during measurement; the actual image was used directly. The largest vertical distance between the supraorbital and infraorbital edges was used to calculate the orbit's height (Coronal section) (Fig. 1A). The largest horizontal distance between the orbit's medial and lateral borders at the superficial level of the frontozygomatic suture was used to calculate the orbit's width (Coronal section) (Fig. 1A). The shortest perpendicular distance between the midpoint of the optic canal's starting and the line joining the orbit's lateral and medial margins at the level where the optic nerve was constantly traced was used to calculate the orbit's depth (axial section) (Fig. 1B). Dimensions of the orbit's lateral and medial borders (axial section): The medial wall length was determined by measuring the distance between the anterior corner of the me-dial wall and the anteromedial point of the optic canal (Fig. 1C), and the lateral wall length was determined by measuring the distance between the anterior corner of the lateral wall and the anterolateral edge of the fissura orbitalis superior (Fig. 1D). The size of the closed bone line that was drawn after the foramen supraorbitale, anterior border of the fossa lacrimalis, frontozygomatic suture, and infraorbital margins was automatically calculated using software to determine the orbital opening area (Coronal section) (Fig. 1E).

Interorbital width (Coronal section): Fig. 2A shows the measurement of the separation between the two dacryon points on the orbital apertures' medial borders. Biorbital width (Coronal section): Fig. 2B shows the distance between the most conspicuous points of the left and right orbits' lateral margins. The distance between the most protruding sites anterior to the right and left zygomatic bones was used to determine the bimalar (interzygomatic) width (Coronal section) (Fig. 2C). Skull transverse diameter (axial section): The transverse diameter of the skull was measured between the furthest locations after the section with the biggest transverse diameter was taken (Fig. 2D). Axial section of the optic nerve-sheath width: The width of the optic nerve and its sheath was measured at the point where it seemed to be thickest (Fig. 2E).

Data analysis with machine learning algorithms and artificial neural networks

Machine learning is an artificial intelligence method that enables computers to learn from experience, without explicit programming. Using a variety of techniques, it enables pattern identification, classification, and prediction in big datasets. Supervised learning, unsupervised learning, and reinforcement learning are the three primary categories into which machine learning is usually separated.

Supervised learning is an approach that builds a model by establishing a relationship between the input and output in the dataset. Un-supervised learning aims to discover hidden patterns and features in data without any prior labeled information. The reinforcement learning model is a method that rein-forces the matching of inputs and outputs such that the system can reach the correct outputs[16].

Several classification algorithms were used in this study. The Decision Tree (DT) algorithm is a fast, efficient, and commonly used method that partitions data recursively. Logistic Regression (LR) utilizes a sigmoid function to model the probability of class membership. Random Forest (RF) is an ensemble technique based on the generation of multiple decision trees. The Extra Tree Classifier (ETC), an advanced variant of RF, achieves better performance by introducing randomness in node splitting and utilizing the entire training data. Linear Discriminant Analysis (LDA) identifies linear combinations of features that best separate multiple classes[16].

Artificial Neural Networks (ANNs) are mathematical models inspired by the learning processes of the human brain, capable of analyzing complex data patterns through a multi-layered structure. A typical ANN consists of an input layer, one or more hidden layers, and an output layer. During training, the network learns the mapping between input data and corresponding outputs. After training, its performance is evaluated on previously unseen data[16].

Machine learning (ML) algorithms and artificial neural networks (ANN) were implemented using a Monster Abra A7 V12.5 model i5 operating system computer. Random Forest (RF), Decision Tree (DT), Logistic Regression (LR), Extra Tree Classifier (ETC), Linear Discriminant Analysis (LDA), Quadratic Discriminant Analysis (QDA), Gaussian Naive Bayes (GaussianNB), k-nearest neighbors (k-NN) algorithms were preferred among ML algorithms and Multilayer perceptron classifier (MLCP) was preferred among ANN algorithms. For ML and MLCP algorithms, 80% of the data was used as training set and 20% as test set. In addition, tenfold cross validation values were also included for the reliability of ML models. For the MLCP model, the input layer consisted of 18 neurons, and the output layer consisted of two neurons and two hidden layers (five neurons in the first layer and ten neurons in the second layer). The data were retrained 100, 500, and 1000 times to ensure that the MLCP topology reflected the reality. Accuracy (Acc), Specificity (Spe), Sensitivity (Sen), F1 score (F1) were used as algorithm performance criteria.

$$Acc = \frac{TP}{TP + FN + FP + TN}$$

$$\mathrm{Sen} = \frac{TP}{TP + FN}$$

$$\mathrm{Spe} = \frac{TN}{TN + FP}$$

$$\mathrm{F1} = 2\frac{Precision \times Recall}{Precision + Recall}$$

Equation 1. (TP; True positive; TN; True negative; FP; False positive; FN; False negative).

ML algorithm analyses were performed using Python 3.9 programming language and scikit-learn 1.1.1 framework, while ANN algorithms were performed using Python 3.9 programming language and TensorFlow framework. The dropout method was used to prevent the ANN model from overlearning and the value was set as 0.05. Among the ML algorithms, maximum depth was set to 5, criterion gini, min-samples-leaf 2, n-estimators 100, min-samples-split 2, criterion entropy 2, k 5 in the k-NN algorithm. We also evaluated the effects of the parameters on the overall results using the Shapley Additive explanations (SHAP) solver of the RF algorithm.

In this study, the CTGAN methodology was used to evaluate changes in accuracy values that may arise from the number of data points. GTGAN is a type of Generative Adversarial Network (GAN) and is a synthetic data generation method used for tabular, i.e., numerical data. This newly generated data exhibits characteristics similar to real data. This model is fundamentally built on two main components: the generator and the discriminator. The generator component produces synthetic data, while the discriminator component regulates how accurately this newly generated data reflects reality. This synthetic data generation method is used in situations where the amount of data is limited[35,36].

In the study, the CTGAN model was used to increase the number of original data points, and the number "n" was increased to "2n." This means that 180 additional synthetic data points were created. During model training, a batch size of 32 was used, and the epoch was set to 1000. The random noise vector size was 100, the number of hidden layers was 3, and the LeakyRELU function was used for hidden layer activation.

Basic statistical analysis

The conformity of the parameters to the normal distribution was tested using the Anderson–Darling test. Mean standard deviation values for the data conforming to a normal distribution and median (minimum–maximum) values for the parameters not conforming to a normal distribution were included. The two-sample T test was used for normally distributed data, and the Mann–Whitney U test was used for non-normally distributed data. The Minitab 17 package program was used for basic statistical analyses.

Data availability

The datasets used and/or analyzed during the current study available from the corresponding author on reasonable request.

Received: 5 August 2025; Accepted: 18 November 2025
Published online: 29 November 2025

References

1. Utkualp, N. & Ilker, E. Anthropometric measurements usage in medical sciences. *BioMed. Res. Int.* **2015**, 404261 (2015).
2. Mohajan, D. & Mohajan, H. K. Body mass index (BMI) is a popular anthropometric tool to measure obesity among adults. *J. Innov. Med. Res.* **2**, 25–33 (2023).
3. Oliveira, M. A. M. D., Fagundes, R. L. M., Moreira, E. A. M., Trindade, E. B. S. D. M. & Carvalho, T. D. Relation between anthropometric indicators and risk factors for cardiovascular disease. *Arq. Bras. Cardiol.* **94**, 478–485 (2010).
4. Rezakhaniha, S., Rezakhaniha, B. & Siroosbakht, S. Which of the anthropometric parameters and hormonal variables in prepubertal children are correlated to true micropenis. *Iran J. Pediatr.* **31**, e108534 (2021).
5. Kaashki, N. N., Hu, P. & Munteanu, A. Deep learning-based automated extraction of anthropometric measurements from a single 3-D scan. *IEEE Trans. Instrum. Meas.* **70**, 1–14 (2021).
6. Demir, M. et al. Craniofacial morphometry of schizophrenia patients. *Anna. Health Sci. Res.* **6**, 10–18 (2017).
7. Dabiri, M. et al. Neuroimaging in schizophrenia: A review article. *Front. Neurosci.* **16**, 1042814 (2022).
8. Silverstein, S. M. et al. Retinal microvasculature in schizophrenia. *Eye Brain* **13**, 205–217 (2021).
9. American Psychiatric Association. Diagnostic and Statistical Manual of Mental Disorders in *DSM- 5* (ed. American Psychiatric Association) (Washington DC, 2013).
10. Orsolini, L., Pompili, S. & Volpe, U. Schizophrenia: A narrative review of etiopathogenetic, diagnostic and treatment aspects. *J. Clin. Med.* **11**, 5040 (2022).
11. Trifu, S. C., Kohn, B., Vlasie, A. & Patrichi, B. E. Genetics of schizophrenia (Review). *Exp. Ther. Med.* **20**, 3462–3468 (2020).
12. Fatemi, S. H. & Folsom, T. D. The neurodevelopmental hypothesis of schizophrenia, revisited. *Schizophr. Bull.* **35**, 528–548 (2009).
13. Eyles, D. W. How do established developmental risk-factors for schizophrenia change the way the brain develops?. *Transl. Psychiatry* **11**, 158 (2021).
14. Francies, O., Makalanda, L., Paraskevopolous, D. & Adams, A. Imaging review of the anterior skull base. *Acta Radiol. Open.* **7**, 2058460118776487 (2018).
15. Grech, R. et al. Imaging of adult ocular and orbital pathology—A pictorial review. *J. Radiol. Case Rep.* **8**, 1–29 (2014).
16. Toy, S. et al. A study on sex estimation by using machine learning algorithms with parameters obtained from computerized tomography images of the cranium. *Sci. Rep.* **12**, 4278 (2022).
17. Horga, G. et al. Correlations between ventricular enlargement and gray and white matter volumes of cortex, thalamus, striatum, and internal capsule in schizophrenia. *Eur. Arch. Psychiatry Clin. Neurosci.* **261**, 467–476 (2011).
18. Pearlson, G. D. & Marsh, L. Structural brain imaging in schizophrenia: A selective review. *Biol. Psychiatry.* **46**, 627–649 (1999).
19. Wheeler, A. L. & Voineskos, A. N. A review of structural neuroimaging in schizophrenia: from connectivity to connectomics. *Front. Hum. Neurosci.* **8**, 653 (2014).
20. Keser, S., Yıldız, S. & Emre, E. A morphometric examination of the orbita structure in schizophrenia patients: A retrospective study. *Med. Rec.* **7**, 195–200 (2024).
21. Howes, O. D., Cummings, C., Chapman, G. E. & Shatalina, E. Neuroimaging in schizophrenia: An overview of findings and their implications for synaptic changes. *Neuropsychopharmacology* **48**, 151–167 (2023).
22. Boyes, J., Whalley, H. C., Lawrie, S. M., Johnstone, E. C. & Best, J. J. A MRI study of ocular hypertelorism in individuals at high risk of developing schizophrenia. *Schizophr. Res.* **50**, 1–2 (2001).
23. Lawrie, S. M. et al. Neurodevelopmental indices and the development of psychotic symptoms in subjects at high risk of schizophrenia. *Br. J. Psychiatry* **178**, 524–530 (2001).
24. Green, M. F., Bracha, H. S., Satz, P. & Christenson, C. D. Preliminary evidence for an association between minor physical anomalies and second trimester neurodevelopment in schizophrenia. *Psychiatry Res.* **53**, 119–127 (1994).
25. Nielsen, A. N., Barch, D. M., Petersen, S. E., Schlaggar, B. L. & Greene, D. J. Machine learning with neuroimaging: Evaluating its applications in psychiatry. *Biol. Psychiatry Cogn. Neurosci. Neuroimaging.* **5**, 791–798 (2020).

26. Lai, J. W., Ang, C. K. E., Acharya, U. R. & Cheong, K. H. Schizophrenia: A survey of artificial intelligence techniques applied to detection and classification. *Int. J. Environ. Res. Public Health.* **18**, 6099 (2021).
27. Davatzikos, C. Machine learning in neuroimaging: Progress and challenges. *Neuroimage* **197**, 652 (2019).
28. Zhang, Z., Li, G., Xu, Y. & Tang, X. Application of artificial intelligence in the MRI classification task of human brain neurological and psychiatric diseases: A scoping review. *Diagnostics (Basel)* **11**, 1402 (2021).
29. Durstewitz, D., Koppe, G. & Meyer-Lindenberg, A. Deep neural networks in psychiatry. *Mol. Psychiatry* **24**, 1583–1598 (2019).
30. Zhang, J. et al. Detecting schizophrenia with 3D structural brain MRI using deep learning. *Sci. Rep.* **13**, 14433 (2023).
31. Deniz, S. et al. Gender estimation from morphometric measurements of mandibular lingula by using machine learning algorithms and artificial neural networks. *Niger J. Clin. Pract.* **27**, 732–738 (2024).
32. Senol, G. T., Kürtül, I., Ray, A. & Ray, G. Machine learning algorithms for sex classification by using variables of orbital structures: A computed tomography study. *Int. J. Morphol.* **42**, 970–976 (2024).
33. Triantafyllou, G. et al. Sex estimation through orbital measurements: a machine learning approach for forensic science. *Diagnostics (Basel)* **14**, 2773 (2024).
34. Shen, D., Wu, G. & Suk, H. Deep learning in medical image analysis. *Annu. Rev. Biomed. Eng.* **19**, 221–248 (2017).
35. Xu, L., Skoularidou, M., Cuesta-Infante, A., & Veeramachaneni, K. Modeling tabular data using conditional gan. Advances in neural information processing systems, 32 (2019).
36. Alqulaity, M. & Yang, P. Enhanced conditional GAN for high-quality synthetic tabular data generation in mobile-based cardiovascular healthcare. *Sensors* **24**(23), 7673 (2024).

Acknowledgements

Our profound appreciation goes out to Prof. Dr. Hanefi Yıldırım for his in-valuable assistance in supplying and disseminating the radiological images utilized in this investigation.

Author contributions

Conceptualization, E.E., D.O.S. and S.A.; methodology, E.E. and Y.S..; software, Y.S.; formal analysis, E.E., S.S.K. and O.K.; investigation, E.E., D.O.S .and S.A.; resources, E.E., S.S.K., D.O.S; data curation, SA, Y.S.; writing-original draft preparation, E.E.; writing-review and editing, S.A., O.K. and S.S.K. All authors have read and agreed to the published version of the manuscript.

Declarations

Competing interests

The authors declare no competing interests.

Additional information

Correspondence and requests for materials should be addressed to S.A.